UDK 620.1:620.3:679.7.022.4
Original scientific article/Izvirni znanstveni članek

ISSN 1580-2949
MTAEC9, 55(2)293(2021)

ISOTHERMAL CURING KINETICS OF POLYMETHACRYLIMIDE/NANO-SiO_2 COMPOSITES BASED ON A DYNAMIC THERMOMECHANICAL ANALYSIS

IZOTERMALNA KINETIKA UTRJEVANJA POLIMETAKRILIMIDA/NANO-SiO_2 KOMPOZITOV NA OSNOVI DINAMIČNE TERMOMEHANSKE ANALIZE

Jing Zhang[1,2,3*], Yi-min Wu[1], Xu Ma[1], Bao-Yu Huang[2], Song Lv[2], Jia-xing Jiang[3], Ji-Jun Tang[1]

[1]School of Materials Science and Engineering, Jiangsu University of Science and Technology, Zhenjiang 212003, Jiangsu, China
[2]Changzhou Sveck Photovoltaic New Material Co., Ltd, Changzhou 213200, Jiangsu, China
[3]Wuxi Jiefu Electroacoustic Co., Ltd, Wuxi 214192, Jiangsu, China

Prejem rokopisa – received: 2020-09-25; sprejem za objavo – accepted for publication: 2020-11-12

doi:10.17222/mit.2020.191

The isothermal curing kinetics of polymethacrylimide/nano-SiO_2 composites were investigated using a dynamic thermomechanical analysis. The relative conversion was defined with the storage modulus. The Avrami model-fitting method, Friedman method and integral method were applied to analyze the curing kinetics. The storage modulus and loss modulus increased appreciably, spanning three orders of magnitude throughout the curing. The frequency correlation of the relative conversion was noticeable at 180 °C because the glass transition took place when the curing degree was not high enough. The Avrami model-fitting analysis gave good fits for the experimental data. The activation energy calculated with the Avrami equation changed from 65.46 kJ/mol to 25.28 kJ/mol at 180–190 °C, while at 190–200 °C, the activation energy changed from 107.14 kJ/mol to 63.82 kJ/mol. The model-free analysis revealed the dependence of the activation energy on the relative conversion. The activation energy increased from 104.3 kJ/mol to 130.6 kJ/mol with the use of the Friedman method when the relative conversion ranged between 0.4–0.8. Similarly, the activation energy calculated with the integral method increased from 71.5 kJ/mol to 103.4 kJ/mol. When the relative conversion exceeded 0.8, the activation energy decreased gradually. The mobility of the reactive groups was hindered and the crosslinking density of the composite was much higher. The curing kinetics became diffusion controlled. The activation energy of the PMI/SiO_2 composite was greater than that of PMI, which could be attributed to the hindrance effect caused by nano-SiO_2.

Keywords: polymethacrylimide, SiO_2, nanocomposites, isothermal curing, dynamic thermomechanical analysis (DMA)

Avtorji članka so z dinamično termomehansko analizo (DMA) raziskovali izotermno kinetiko utrjevanja kompozitov na osnovi polimetakrilimida in nano-SiO_2. Relativno pretvorbo so definirali z modulom shranjene energije. Za analizo kinetike utrjevanja so uporabili Avramijev model prilagoditve ter Friedmanovo- in integralno metodo. Modula shranjene energije in izgub sta med utrjevanjem znatno naraščala (za tri velikostne razrede) s povečevanjem izmenične obremenitve. Opazili so pomembno povezavo med frekvenco in relativno pretvorbo pri 180 °C, ker takrat prihaja do prehoda iz steklaste faze, ko stopnja utrjevanja še ni dovolj velika. Analiza z Avramijevim modelom prilagoditve je pokazala dobro ujemanje z eksperimentalnimi podatki. Aktivacijska energija izračunana z Avramijevo enačbo se je spremenila s 65,46 kJ/mol na 25,28 kJ/mol med 180 °C in 190 °C. Medtem, ko se je med 190 °C in 200 °C spremenila s 107,14 kJ/mol na 63,82 kJ/mol. Avtorji so s pomočjo modelne proste analize odkrili odvisnost med aktivacijsko energijo in relativno pretvorbo. S Friedmanovo metodo določena aktivacijska energija je narasla s 104,3 kJ/mol na 130,6 kJ/mol, medtem ko je bila relativna pretvorba v območju med 0,4 in 0,8. Podobno je aktivacijska energija izračunana z integralno metodo narasla z 71,5 kJ/mol na 103,4 kJ/mol. Aktivacijska energija je začela postopoma padati, ko je relativna pretvorba presegla vrednost 0,8. Mobilnost reaktivnih skupin je bila zavrta in gostota prečnega veriženja kompozita je bila mnogo večja. Kinetika utrjevanja je postala mnogo bolj difuzijsko kontrolirana. Aktivacijska energija PMI/SiO_2 kompozita je bila večja kot aktivacijska energija samega PMI, kar avtorji pripisujejo vplivu zadrževalnega učinka nano-SiO_2, ki delujejo kot ovire.

Ključne besede: polimetakrilimid, SiO_2, nanokompoziti, izotermalno utrjevanje, dinamična termomehanska analiza (DMA)

1 INTRODUCTION

Polymethacrylimide (PMI) foam is a high-performance thermosetting material developed by Degussa in 1972. It is usually prepared by heat treating block copolymers of methacrylonitrile (MAN) and methacrylic acid (MAA) in the presence of crosslinking agents and foaming agents.[1–3] PMI foam is a completely closed-cell polymer foam with a high cell wall/volume ratio.[4,5] The molecular chains contain imide rings with excellent thermal stability, as shown in **Figure 1**. Since the invention of PMI foam, great efforts have been made to study the preparation methods, structures, properties and applications of PMI.[5–9] Compared with other foam materials, PMI foam is known to have excellent mechanical properties, a high stiffness-to-weight ratio and thermal resistance. As the lightweight core material for sandwich structures, PMI foam has been applied widely in military and security, aerospace and aeronautics, railcar manufacturing and automotive industry.[10–15]

*Corresponding author's e-mail:
zhangjing@just.edu.cn (Jing Zhang)

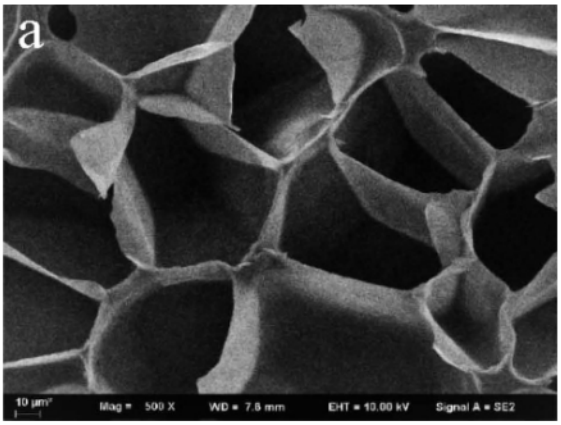

b

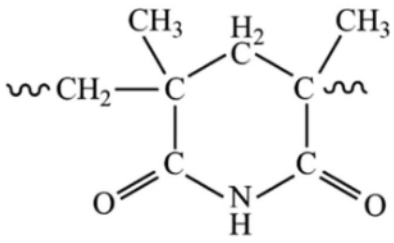

Figure 1: a) SEM image of the PMI-foam morphology and b) the six-member imide ring in a molecule chain

However, it cannot be neglected that the cost of MAN raw materials is high. And the mechanical properties of PMI foam degrade with a decrease in the density. During the past decades, the candidate of the expensive MAN, acrylonitrile (AN), was excavated to prepare PMI foam to reduce the cost.[6,9,16] Some inorganic nanofillers were taken as the reinforcing materials or flame retardants to enhance the comprehensive properties of PMI foam.[17,18] The development of the PMI composite has attracted increasing attention in recent years. By introducing inorganic nanofillers, a new PMI foam with a low cost and high performance has been obtained successfully.[17,18] It was reported that the uniform dispersion of nano-SiO_2 plays an important role in promoting the mechanical properties of thermosetting nanocomposites.[19–21] Z. Zhang et al.[22] found that the thermal stability and flexural strength of PMI/SiO_2 composites were improved because of an addition of silicates. Moreover, highly reactive nanoparticles can affect the curing behavior in a thermosetting system.[23] S. Ghiyasia et al.[19] found that the introduction of modified SiO_2 could facilitate the crosslinking of epoxy/amine system thanks to the abundance of amine reactive groups on the particle surface. Therefore, the research on the PMI/SiO_2 nanocomposite has an important significance and application prospect.

Almost all the properties of a high-performance foam depend on the three-dimensional network formed by a chemical reaction.[24] The role of nanofillers in the promotion of the properties of thermosetting materials was detected by a detailed curing-kinetics analysis based on calorimetric studies.[25–27] The curing-kinetics parameters related to the network formation can provide substantial information concerning the structure, properties and also the processability of PMI. The kinetic parameters of thermosetting materials are typically obtained with differential scanning calorimetry (DSC). However, it should be noted that the liberation of heat throughout the curing is too slight to be detected. Besides, a series of polycondensation, which can release small molecules, takes place during the curing. A baseline drift can be found with DSC because of the weight change of the samples. On the other hand, the dynamic thermomechanical analysis (DMA) is a very important tool that can precisely monitor the motions of polymer chains, including localized transitions such as side-chain movements.[28,29] By comparison, the DMA is a more powerful and suitable tool for measuring transitions during the curing of PMI. In our previous work, the isothermal curing of PMI was investigated with the DMA.[30]

In this article, PMI/SiO_2 nanocomposites were prepared using AN, MAA and nano-SiO_2 via radical bulk copolymerization. A series of isothermal-curing experiments were carried out using the DMA at 180–200 °C. The relative conversion was defined by the storage modulus. Hsich's non-equilibrium thermodynamic fluctuation theory, the Avrami model-fitting method, differential and integral isoconversional methods were employed to quantify the isothermal curing process. The quantitative analysis helps us establish the quantitative relation between the curing conditions and the properties of PMI/SiO_2 nanocomposites to reduce the experiments in order to optimize the curing process.

2 EXPERIMENTAL PART

2.1 Materials

AN of analytical grade was supplied by Sinopec QiLu Petrochemical Company (China). MAA of analytical grade was offered by Sinopharm Chemical Reagent Co. Ltd. (China). The nano-SiO_2 with a particle size of 15 nm (S104597) was provided by Aladdin Industrial Corporation (China). Azobisisobutyronitrile (AIBN) supplied by Shanghai Macklin Biochemical Co. Ltd. (China) was used as the initiator. Acrylamide (AM) purchased from Sinopharm Chemical Reagent Co. Ltd. (China) was selected as the cross-linking agent. The starting materials were high-purity substances, used as received without further purification.

2.2 Preparation of the composite board

The preparation of the PMI/SiO_2 composite board was carried out via radical bulk copolymerization. Firstly, the mixture of 110 g AN, 90 g MAA, 1 g AIBN,

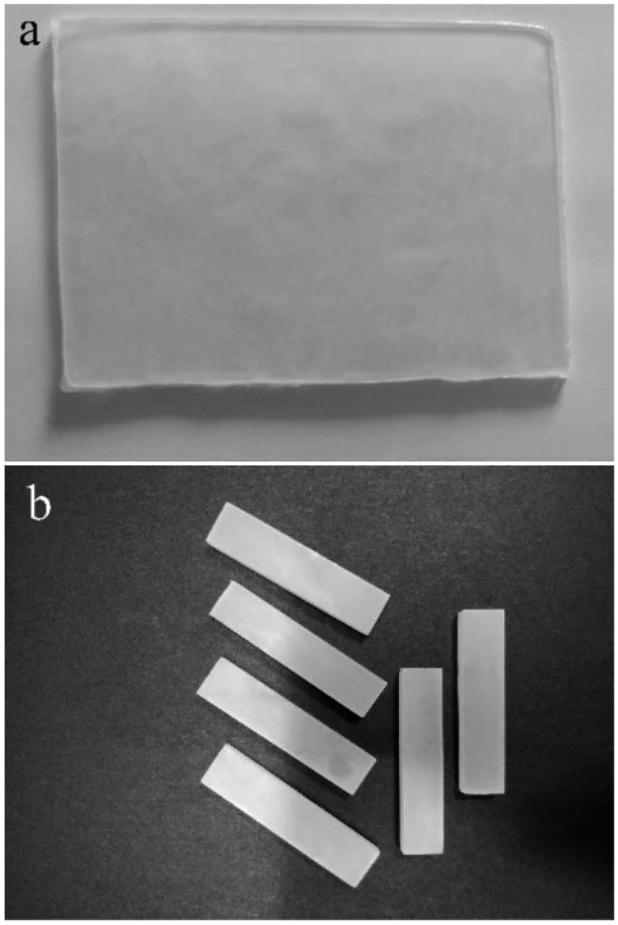

Figure 2: a) PMI/SiO_2 composite board and b) the samples cut from the board

3 g AM, and 6.12 g SiO_2 were pre-polymerized in a three-necked flask in a water bath at 70 °C for 100 min. Secondly, the prepolymer was poured into a vitreous mold having dimensions of 210.0×120.0×5.0 mm. Afterward, the mold was sunk into the water bath at 60 °C for 72 h. Finally, the PMI/SiO_2 composite board was obtained. The samples cut from the composite board with a mechanical cutter were made into rectangular strips having dimensions of 45.0×10.0×4.0 mm. **Figure 2** shows the PMI/SiO_2 composite board and the samples from the experiment.

2.3 Measurement

The isothermal curing experimental tests were carried out using a DMA (242C, NETZSCH, Germany). The specimens were heated up from room temperature at a heating rate of 3 °C/min under an air atmosphere. Isothermal curing was conducted for 10 h at five different temperatures (180, 185, 190, 195 and 200) °C, respectively. The oscillation frequency of the experiment was set to (0.1, 0.333, 1, 3.333 and 10) Hz in the three-point bending mode with a 30 μm amplitude.

3 RESULTS AND DISCUSSION

3.1 Isothermal-curing characterization

Figure 3 shows the isothermal-curing curves of the PMI/SiO_2 nanocomposite at 180 °C. The evolution of dynamic mechanical properties can be divided into three stages. In the first stage, the temperature rapidly increased from room temperature to the preset curing temperature. The heating process corresponded to the softening of the specimens. The storage modulus (E') and the loss modulus (E'') decreased rapidly to the minimum in this stage, while the loss factor (tan δ) increased initially and then decreased, forming a peak corresponding to the rapid decline period of E'. In the second stage, E' and E'' underwent a slow increase at first and then increased appreciably, spanning three orders of magnitude. In the rapid growth phase of E' and E'', the imidization involving acid and nitrile units of the copolymers took place and a large number of hexahydric imide rings were formed (**Scheme 1**).[5–7]

There were two peaks on the curve of tan δ in the second stage. The first peak (at a time of 136.6 min) was relatively weak and might have corresponded to the crosslinking reactions, including the deamination between -NH_2 groups (**Scheme 2**), the dehydration between -NH_2 and -COOH groups (**Scheme 3**), and the dehydration crosslinking adjacent to -COOH groups (**Scheme 4**).[5] The second peak (at a time of 190.5 min) appeared in the rapid growth period of E' and E'', corresponding to the imidization shown as **Scheme 1**. Obviously, the second stage was the main curing of the

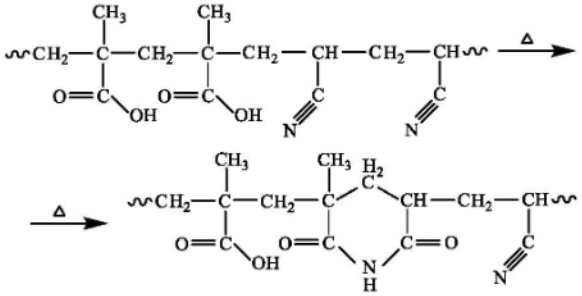

Scheme 1: Cyclization reaction in the molecule chain of PMI

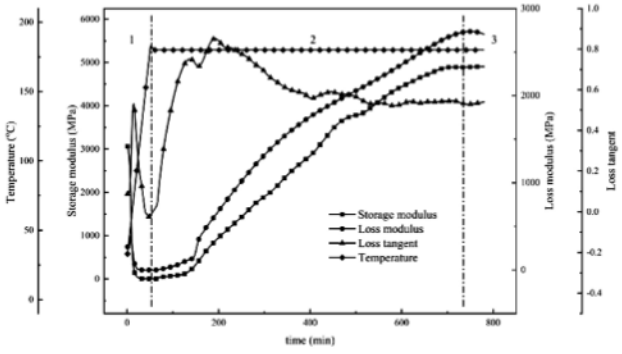

Figure 3: DMA isothermal measurement of PMI/SiO_2 nanocomposite at 180 °C

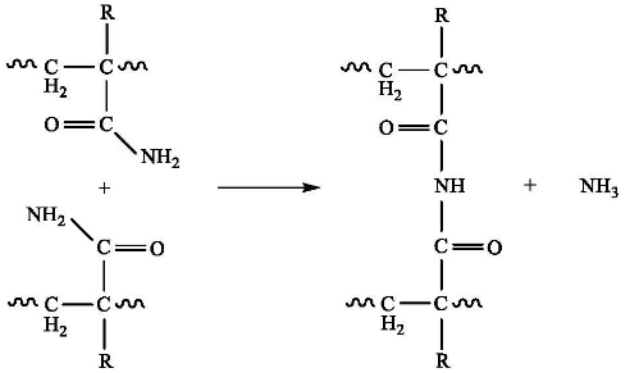

Scheme 2: Deamination reaction of AM and other molecules

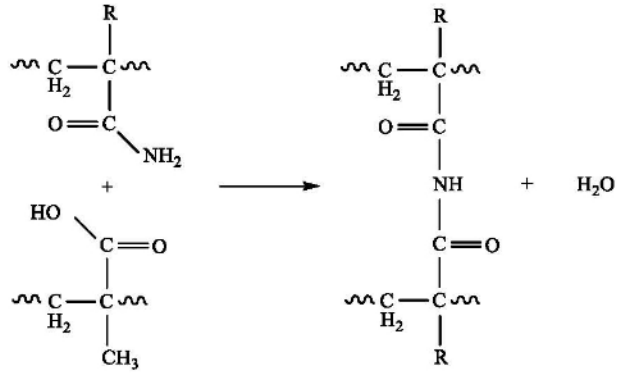

Scheme 3: Dehydration reaction of AM and other molecules

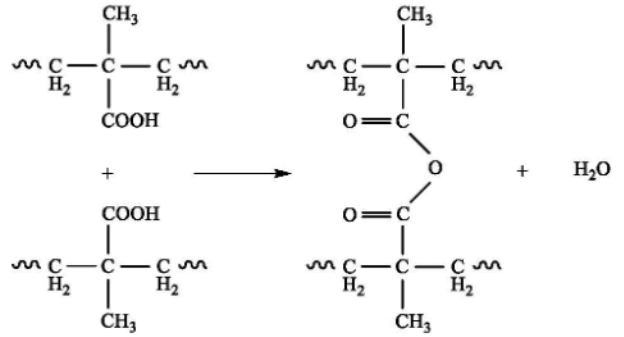

Scheme 4: Dehydration crosslinking reaction of MAA and adjacent molecules

PMI/SiO_2 composite. When the reaction proceeded to the third stage, the changes of E', E'' and tan δ tended to slow down, ultimately reaching the equilibrium. It can be concluded that the isothermal curing of the PMI/SiO_2 nanocomposite was over and the composite was completely cured in the end.

Figure 4 shows the isothermal-curing curves of the PMI/SiO_2 nanocomposite at 200 °C. Compared with the curves at 180 °C from **Figure 3**, the growth rate of E' and E'' in the second stage was much higher. This is due to the fact that a higher temperature is more conducive to the segmental motion. Moreover, a sharp peak (at a time of 110.8 min) appeared on the curve of tan δ in the second stage. It might have corresponded to the crosslinking of the adjacent -CN groups, which could form a cyclic

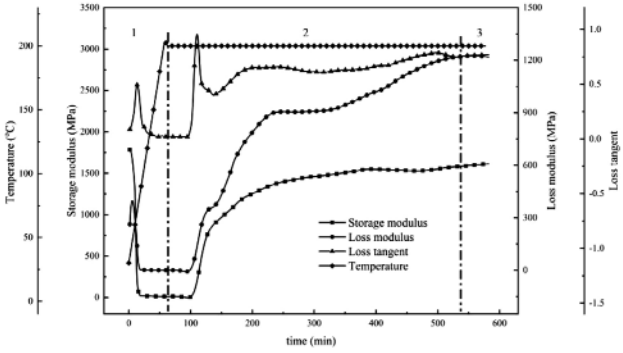

Figure 4: DMA isothermal measurement of PMI/SiO_2 nanocomposite at 200 °C

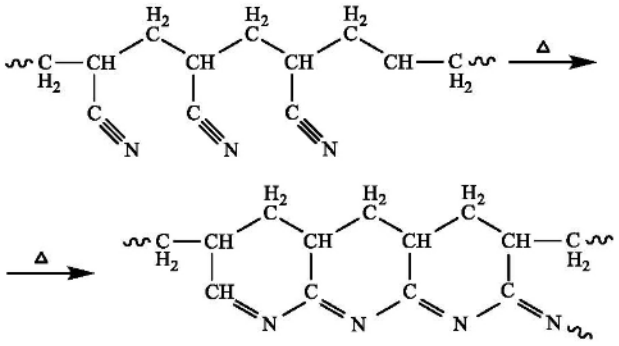

Scheme 5: Intermolecular crosslinking reaction of AN units

polyimine structure, namely "a ladder polymer" (**Scheme 5**).[31]

In order to quantify the growth of dynamic mechanical properties during the curing of the PMI/SiO_2 nanocomposite, the relative conversion defined by E' is indicated as follows:[32]

$$\alpha' = \frac{(E'_t - E'_0)}{(E'_\infty - E'_0)} \quad (1)$$

where α' is the relative conversion, E'_0 is the storage modulus at the initial time, E'_t is the storage modulus at

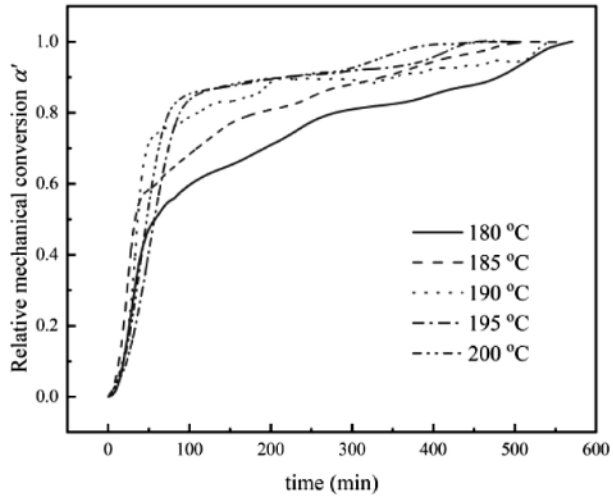

Figure 5: Relative-conversion curves of PMI/SiO_2 nanocomposite at different temperatures

a specified time during the curing, and E'_∞ is the storage modulus at the infinite time. In this study, the starting point in the second stage was considered as the initial time and the final equilibrium value of the curing in the third stage was recognized as the ending point of E'.

Figure 5 depicts the curves of relative conversion as a function of time at various curing temperatures. The isothermal curing of the PMI/SiO_2 nanocomposite follows the typical path of thermosetting materials including a rapid increase in the reaction rate and higher temperatures. Otherwise, a higher curing temperature results in a higher reaction rate at a given conversion. Moreover, the major growth stage of the relative conversion advanced with the increase in the curing temperature. It is worth mentioning that the growth mode of the relative conversion can be divided into two categories, including the low-temperature range (180–185 °C) and the high-temperature range (190–200 °C). In the low-temperature range, the growth of the relative conversion underwent a transition stage where the growth rate of conversion was relatively slow. On the other hand, in the high-temperature range, no transition stage was observed, indicating that the growth mechanism of E' varied at different temperatures. In order to find the inner cause for the dissimilarity between different temperature ranges, a multiple-frequency isothermal curing test was carried out at 180 °C and 200 °C, respectively.

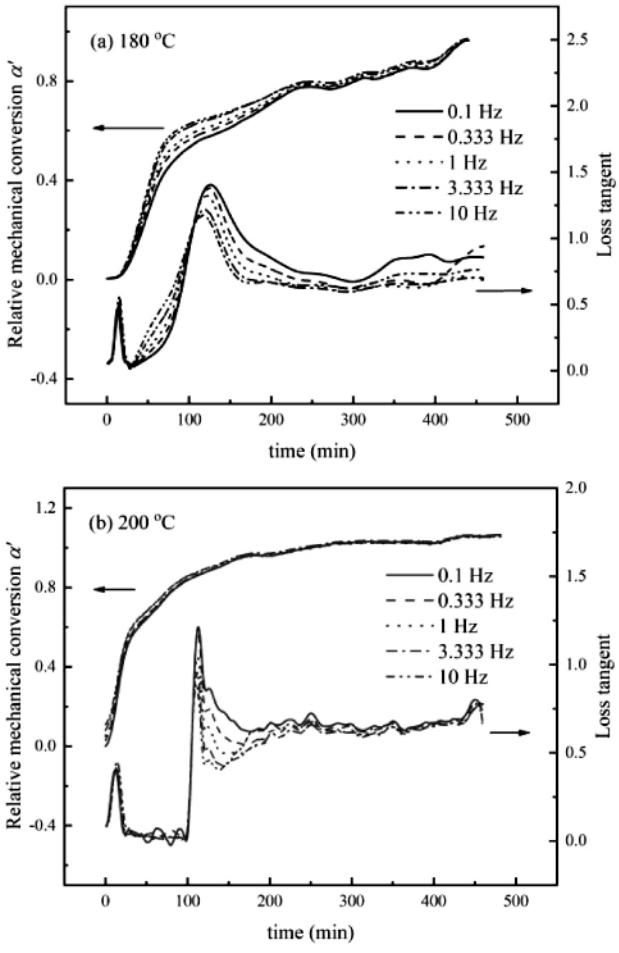

Figure 6: Mult-frequency conversion curves and tan δ curves of PMI/SiO_2 at: a) 180 °C and b) 200 °C

Figure 6 shows the multi-frequency conversion curves and the corresponding tan δ curves of the PMI/SiO_2 composite at different temperatures. Obviously, the multi-frequency conversion curves separate in the middle transition stage at 180 °C, but overlap with each other at the prophase and anaphase of the process. With a decrease in the frequency, the values of conversion corresponding to the same time reduce gradually. Moreover, the emergence of peaks on the tan δ curves is delayed with a reduction in the operating frequency. The curves show frequency dependence at low temperatures. However, the multi-frequency conversion curves at 200 °C are independent of the frequency, coinciding together roughly throughout the whole process. The tan δ curves at different frequencies have the same peak position. No frequency correlation is observed at 200 °C. The glass-transition temperature (T_g) of PMI, a thermosetting material, goes up with an increase in the curing degree and cross-linking density below the maximum glass-transition temperature ($T_{g,\infty}$).[33–35] When T_g increases close to the curing temperature (T_c), the system enters the glassy state and the reaction rate reduces sharply. It was pointed out that the glass transition takes place when T_g differs from T_c by 20–30 °C.[32] In this situation, the glass transition is not a temperature point, but a temperature range. The glass transition advances with the increase in the frequency, along with the lower T_g.[36] Therefore, there is a frequency-dependent region on the relative conversion and tan δ curves during the curing of the PMI/SiO_2 composite at 180 °C. At low temperatures, the glass transition takes place when the curing degree of the system is not high enough. In the last stage of curing, the system fully enters the glassy state. However, at 190–200 °C, the curing degree is relatively high and only a small part enters the glassy state at the anaphase. Therefore, the relative-conversion curves show a significant correlation with the frequency at low temperatures, but the frequency correlation is not observed at high temperatures.

3.2 Model-fitting analysis

Hsich derived a new model of curing kinetics based on the concept of the non-equilibrium thermodynamic fluctuation theory of chemical relaxation.[37] It describes the physical or mechanical properties of materials during the curing, which can be represented with Equation (2):

$$\frac{(P_\infty - P_t)}{(P_\infty - P_0)} = \exp\left[-\left(\frac{t}{\tau}\right)^\beta\right] \quad (2)$$

where P represents the mechanical property of the system, β is the chemical-relaxation spectrum width, and τ is the chemical relaxation time.

The Avrami equation was derived using the thermodynamic method for polymer crystallization.[38,39] It was applied to study the curing process of thermosetting resins, such as epoxy resins and thermosetting polyurethanes. The classical form of the Avrami equation can be expressed as follows in Equation (3):

$$1-\alpha = \exp\left[-kt^n\right] \tag{3}$$

where α usually represents the crystallinity of the crystal, k is the kinetic constant depending on the temperature, and n is the Avrami exponent reflecting the crystal growth mechanism and the nucleation behavior of the crystal.

Replacing the mechanical property with the storage modulus and combining it with Equation (1), the Hsich equation can be alternatively written as Equation (4):

$$1-\alpha' = \exp\left[-\left(\frac{t}{\tau}\right)^{\beta}\right] \tag{4}$$

Obviously, Hsich's non-equilibrium thermodynamic fluctuation theory and Avrami's equation have the same formation defining the relative conversion. Applying logarithmic forms to both sides of Equation (3), the following can be obtained:

$$\ln[-\ln(1-\alpha)] = \ln k + n \ln t, \tag{5}$$

By linearly fitting the plot of $\ln[-\ln(1-\alpha')] - \ln t$, kinetic parameters n and k can be obtained from the slope and intercept of the curves at different temperatures, respectively.

Figure 7 presents the $\ln[-\ln(1-\alpha')] - \ln t$ curves of the PMI/SiO_2 nanocomposite at different temperatures. Obviously, the curves can be divided into two segments according to the slope difference. Therefore, each curve should be fitted segmentally. The kinetic parameters calculated with the Avrami equation are listed in **Table 1**. It is evident that the values of n_1 are greater than those of n_2 at each specific temperature. Index n in the Avrami equation reflects the growth mechanism and describes the crystal-growth behavior. Therefore, it is reasonable to conclude that the growth mechanism of conversion varies with the process of isothermal curing.

Table 1: Fitting results of n and k calculated with the Avrami equation at different temperatures

T/°C	180	185	190	195	200
n_1	1.523	1.756	1.782	1.783	1.779
ln k_1	–5.667	–6.215	–6.042	–5.589	–5.110
n_2	0.424	0.321	0.312	0.309	0.422
ln k_2	–1.935	–0.996	–1.359	–1.321	–1.759

Figure 8 shows the fitting curves calculated with the modified Avrami equation. The fitting curves show good agreement with the experimental data, indicating that the Avrami model can accurately predict the evolution of relative conversion of the PMI/SiO_2 composite. It further indicates that the evolution of mechanical properties during the isothermal curing of the PMI/SiO_2 composite is similar to the crystallization of a high polymer.

The empirical correlation between the rate constant and temperature can be illustrated as follows:[29]

$$k^{\frac{1}{n}} = k_0 \exp\left[-\frac{E_a}{RT}\right] \tag{6}$$

where E_a is the activation energy, T is the reaction temperature, R is the universal gas constant and n is the Avrami exponent. The logarithmic form of Equation (6) can be expressed as Equation (7), from which the E_a of the curing can be calculated.

$$\frac{1}{n}\ln k = \ln k_0 - \frac{E_a}{RT} \tag{7}$$

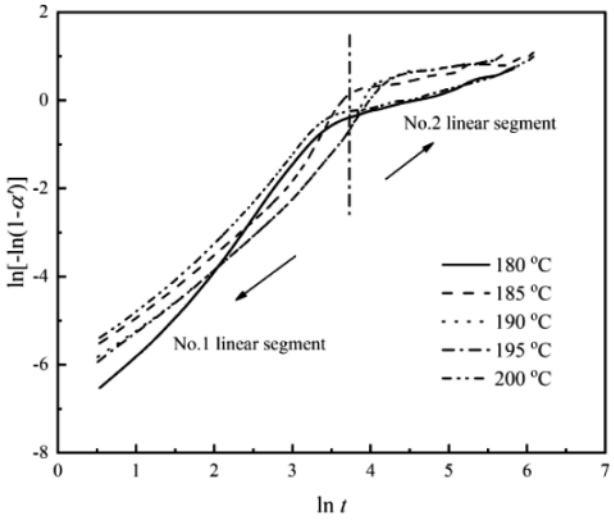

Figure 7: $\ln[-\ln(1-\alpha')] - \ln t$ curves of PMI/SiO_2 at different temperatures

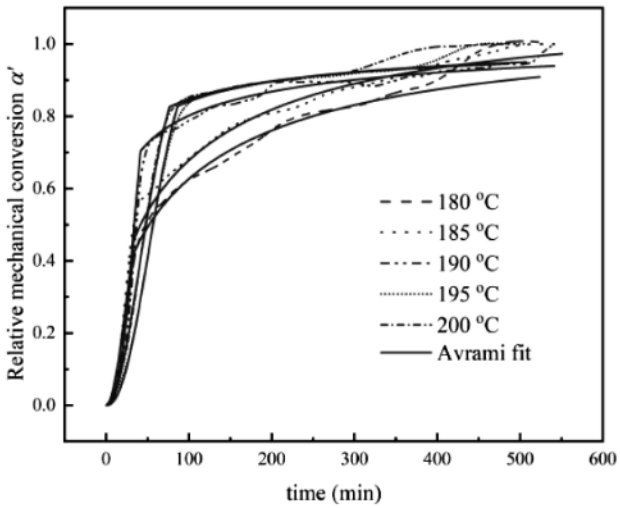

Figure 8: Fitting results of the conversion curves of PMI/SiO_2 with the Avrami equation

Table 2: The k_0 and E_a of PMI/SiO$_2$ composite calculated with the Avrami equation

T/°C	$k_{0,1}$ /min^{-1}	$E_{a,1}$ /kJ·mol^{-1}	$k_{0,2}$ /min^{-1}	$E_{a,2}$ /kJ·mol^{-1}
180–190	5.9×10^4	65.46	8.67	25.28
190–200	1.81×10^9	107.14	8.12×10^2	63.82

Figure 9 illustrates the $(1/n)\ln k - 1/T$ relationship for the linear segments of $\ln[-\ln(1-\alpha')] - \ln t$ in **Figure 7**. The resulting parameters are presented in **Table 2**. It is clearly shown that both $k_{0,1}$ and $k_{0,2}$ at 190–200 °C are greater than their corresponding values at 180–190 °C. This is due to the fact that a higher temperature is more conducive to the segmental motion. The E_a values during the curing in the high-temperature range are greater than the corresponding values in the low-temperature range. Meanwhile, in the same temperature range, the value of $k_{0,1}$ in the first segment is much greater than the value of $k_{0,2}$ in the second segment. A considerable difference in the order of magnitude indicates a transformation from the chemical-control mechanism in the prophase into the diffusion-control mechanism in the anaphase.[37] The decrease in E_a further indicates that the control mechanism was changed during the curing.

Table 3: Activation energy of PMI and PMI/SiO$_2$ during the curing

T/°C	$E_{a,1}$/kJ·mol^{-1}		$E_{a,2}$/kJ·mol^{-1}	
	PMI	PMI/SiO$_2$	PMI	PMI/SiO$_2$
180–190	53.99	65.46	13.96	25.28
190–200	99.81	107.14	41.39	63.82

The activation energy of the PMI/SiO$_2$ nanocomposite during the curing obtained with the Avrami model is given in **Table 3**, together with the E_a for PMI, which was investigated in our previous work.[30] The results show that the E_a of the curing system increases obviously after the incorporation of nano-SiO$_2$, especially in the second stage. This difference can be attributed to the steric hindrance caused by nanoparticles. As the curing progresses, a three-dimensional structure is slowly formed. The SiO$_2$ particles can form crosslinking sites in the network.[34] The crosslinking density of the nanocomposite increases gradually, especially in the later stage. The SiO$_2$ particles anchored in the net structure physically inhibit the segmental motion of PMI chains or even prohibit the curing reactions.[40] In this situation, nano-SiO$_2$ particles act as effective fillers of voids. Moreover, the nanoparticles can modify the microstructure and interface transition zone between the PMI matrix and the nano-SiO$_2$ filler, making the composite denser.[41] Therefore, the increase in the activation energy can be attributed to the hindrance effect caused by SiO$_2$ particles.

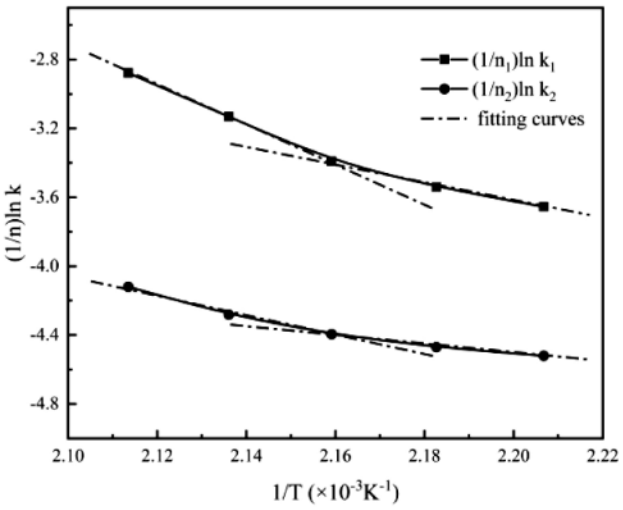

Figure 9: $(1/n)\ln k - 1/T$ relationship for the linear segments of $\ln[-\ln(1-\alpha')] - \ln t$ curves

3.3 Model-free analysis

The complexity of curing involving multiple reactions can be detected with the variable value of the activation energy.[42] Model-free isoconversional methods, including the integral method and differential method, are alternative and advantageous approaches applied to the calorimetric modeling of curing kinetics.[43] With the assumption that both the activation energy and pre-exponential factor are the functions of the degree of curing, both simple and complex chemical reactions are evaluated widely. The significance of the isoconversional method is that no kinetic-rate expression is assumed for the data evaluation.[44,45]

The isothermal-curing kinetics of the PMI/SiO$_2$ composite can be described with the fundamental-rate equation that governs the rate of conversion at a constant temperature as a function of the concentration of the reactants, as shown in Equation (8):

$$\frac{d\alpha}{dt} = k(t) f(\alpha) \tag{8}$$

where α is the conversion, t is the time, $d\alpha/dt$ is the rate of change in conversion, $f(\alpha)$ is the reaction model in accord with the reaction mechanism and $k(T)$ is the reaction-rate constant as a function of temperature due to the Arrhenius equation, as shown in Equation (9):

$$k(T) = A \exp\left(-\frac{E_a}{RT}\right) \tag{9}$$

where A is the frequency factor reflecting the number of collisions between reactive groups, E_a is the activation energy, R is the ideal gas constant and T is the absolute temperature.

Assuming that kinetic parameters E_a and A vary with the extent of the reaction, the Friedman equation can be derived by taking the natural logarithm of both sides of Equation (8):

$$\ln\left(\frac{d\alpha}{dt}\right) = \ln[A_\alpha f(\alpha)] - \frac{E_\alpha}{RT} \tag{10}$$

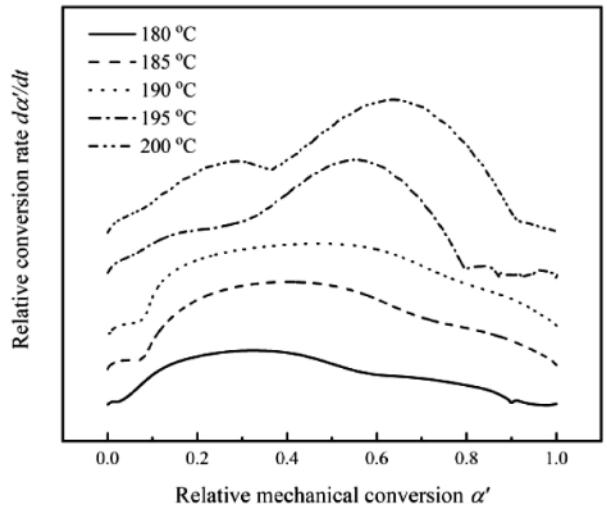

Figure 10: Reaction rate versus relative conversion of PMI/SiO_2

The integral method can be expressed as Equation (11):

$$\ln t_{\alpha,i} = \ln\left[\frac{g(\alpha)}{A}\right] + \frac{E_\alpha}{RT_i} \tag{11}$$

where subscript i represents the ordinal number of the experiment at a constant temperature and $g(\alpha)$ is the integral conversion function of conversion shown in Equation (12):

$$g(\alpha) = \int_0^\alpha \frac{\mathrm{d}\alpha}{f(\alpha)} = A\int_0^{t\alpha} \exp\left(-\frac{E_\alpha}{RT(t)}\right)\mathrm{d}t \tag{12}$$

The isoconversional method comes with the basic assumption that the reaction rate at constant conversion is only the function of temperature. The value of the activation energy can be determined from the slope of ln dα/dt versus 1/T in Equation (10) and ln t versus 1/T in Equation (11) at constant conversion. According to Vyazovkin, the relative conversion rate can be used to calculate the activation energy when the isothermal-curing reaction takes place below $T_{g,\infty}$[46].

For the purpose of modelling parameter determination in Equations (10) and (11), the reaction rate dα'/dt, obtained by differentiating the α'-t curves, as a function of conversion for each temperature is illustrated in **Figure 10**. A similar trend can be observed at 180–190 °C as there is only one major peak on the curves. However, the curves at 195 °C and 200 °C exhibit a noticeable difference as there are two peaks on the curves, implying that the curing mechanism varies at higher temperatures. Therefore, peak separation should be applied with the Gauss fitting method. **Figure 11** shows the Gauss fitting curves of peak separation. The first peak of α' at 0.2–0.3 is marked as Peak 1 and the second peak of α' at 0.5–0.6 is marked as Peak 2. The correlation coefficient R^2 is a parameter used to evaluate the fitting. The closer the R^2 value is to 1, the better is the fitting. As seen from the

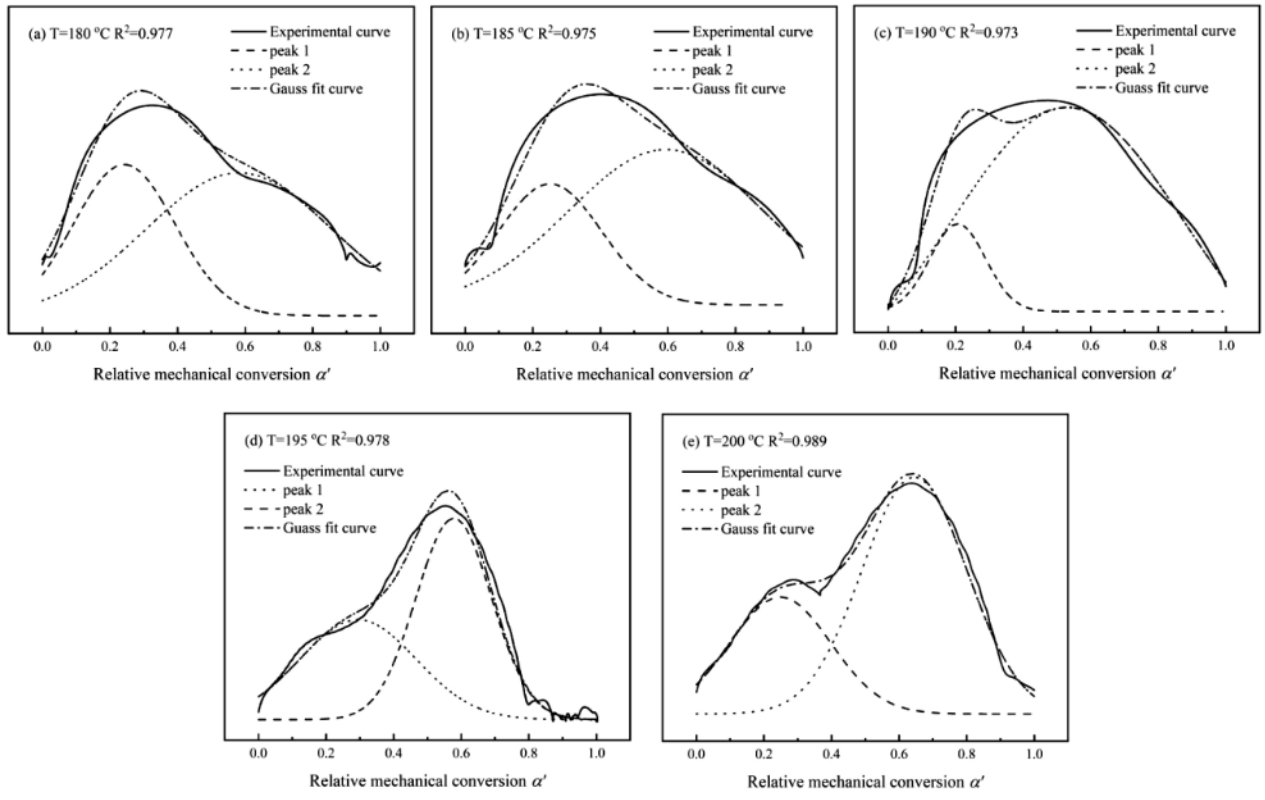

Figure 11: Gauss fitting curves at temperatures of 180–200 °C

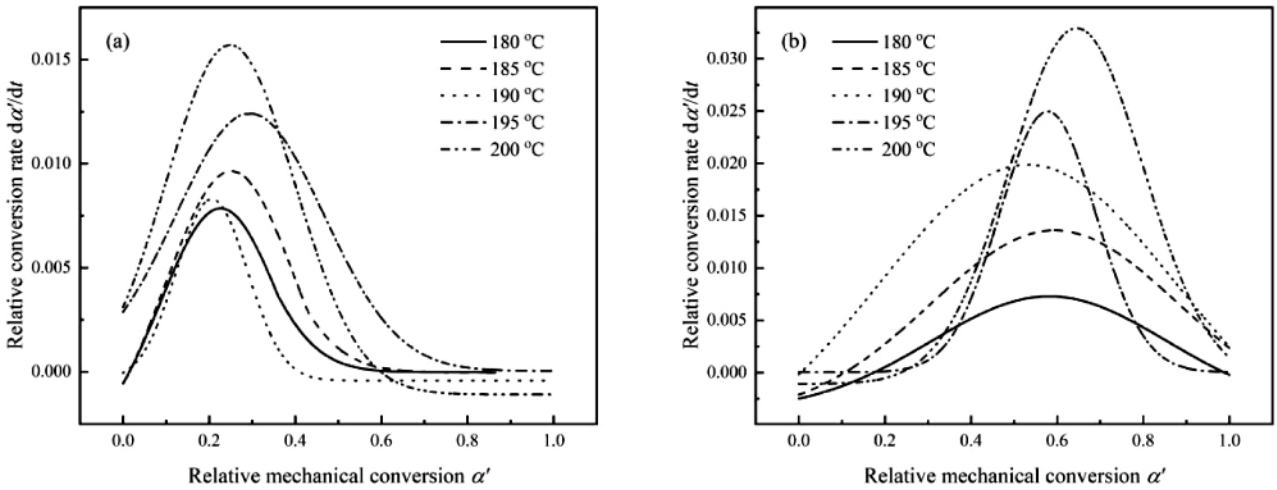

Figure 12: Peak-separation result for the relative reaction rate where: a) is Peak 1 and b) is Peak 2

figures, all the values are above 0.97, indicating that the fitting of the experimental data is satisfactory.

Table 4: Relative conversion at the maximum rate for PMI/SiO_2 composite at different temperatures

T/°C	180	185	190	195	200
α'_{peak1}	0.287	0.354	0.252	0.283	0.249
α'_{peak2}	0.584	0.596	0.537	0.576	0.636

Figure 12 presents the peak-separation result for the relative mechanical conversion rate where **Figure 12a** shows Peak 1 and **Figure 12b** shows Peak 2. Both peaks show an increasing trend with the rise in the curing temperature. **Table 4** summarizes the values of conversion corresponding to the maximum rates of Peak 1 and Peak 2 at different curing temperatures. The results of peak separation are basically in agreement with the common assumption of the isoconversional method. The presence of the two peaks evidences that Peak 2 is the reflection of imidization that takes place at about 0.6 of α', while Peak 1 is the reflection of cross-linking reactions shown in Schemes 2–4. Therefore, focus should be placed on Peak 2 when studying the isothermal curing of the PMI/SiO_2 nanocomposite.

Figure 13 shows the activation-energy curves for isothermal curing obtained with the integral method (a) and Friedman method (b). It should be noted that the values of the slopes are negative when the conversion is less than 0.4 as shown in **Figure 13a**, indicating that the isoconversional methods are not applicable in the early curing stage. Therefore, it is possible to calculate the evolution of E_a when the conversion exceeds 0.4 by linearly fitting the curves as shown in **Figure 13**.

Figure 14 shows the evolution of E_a of the PMI/SiO_2 nanocomposite during the curing in an α' range of 0.4–1.0 obtained with the isoconversional methods. The difference in α' is 0.05. As seen, E_a changed during the whole process, indicating the complexity of the mechanism. Specifically, the initial value of E_a was 104.3 kJ/mol and tended to increase with the curing up to 130.6 kJ/mol in an α' range of 0.4–0.8, as determined with the Friedman method. A similar trend could be ob-

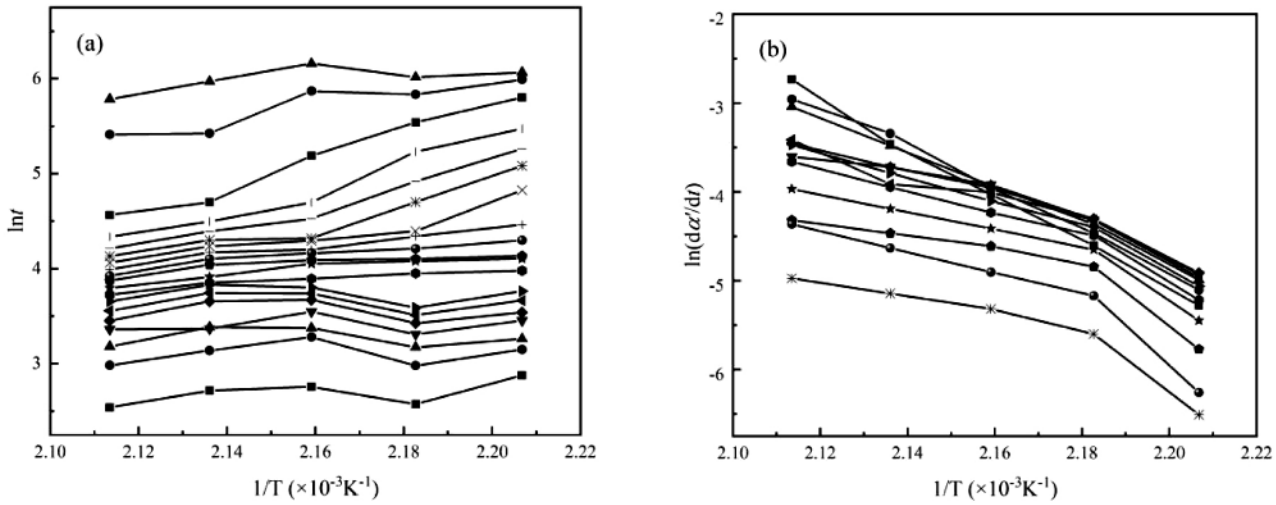

Figure 13: Activation-energy curves for PMI/SiO_2 obtained with: a) the integral method and b) Friedman method

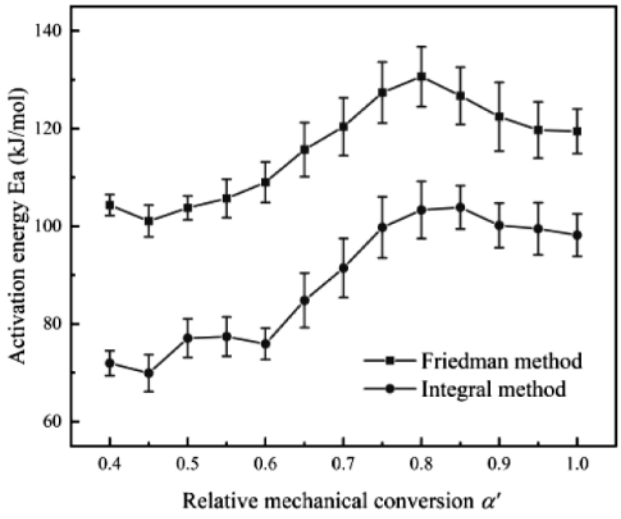

Figure 14: Evolution of E_a during the curing of PMI/SiO_2

served during the use of the integral method when E_a increased from 71.5 kJ/mol to 103.4 kJ/mol. This stage involved the formation of a three-dimensional network through the reactions among polyfunctional groups, including the intermolecular crosslinking of MAA and the crosslinking of AN. The crosslinking density of the system increased gradually with the curing, and the E_a required for the reactions between the reactive functional groups increased. In the later stage of curing when the conversion exceeded 0.8, E_a showed a downward trend. The value of E_a reduced to 119.4 kJ/mol when the Friedman method was used and to 98.2 kJ/mol at the end of curing when the integral method was used. It is noteworthy that a large number of ring structures were formed in the anaphase of curing. The crosslinking density of the composite was much higher and the mobility of the reactive groups was hindered. The kinetics of curing became diffusion controlled, which might have contributed to the reduction in the value of the effective activation energy.

In our previous research on the isothermal curing of PMI, the activation energy ranged between 40–80 kJ/mol at a conversion between 0.4–0.8.[30] It is noteworthy that the E_a of the PMI/SiO_2 composite is much greater than that of PMI during the whole curing. The difference in E_a is probably due to the steric hindrance effect caused by nano SiO_2.This result is in agreement with the analysis made with the Avrami equation, presented in **Table 3**.

4 CONCLUSIONS

A PMI/SiO_2 nanocomposite was prepared from AN, MAA and nano-SiO_2 via radical bulk copolymerization. The isothermal curing of the PMI/SiO_2 nanocomposite was investigated using the DMA at different temperatures. The storage modulus and loss modulus increased appreciably, spanning three orders of magnitude during the curing. The multi-frequency conversion and tan δ curves at 180 °C showed a noticeable frequency correlation. This was due to the fact that the glass transition takes place when the curing degree is not high enough at a low temperature. The Avrami model-fitting analysis gave excellent fits for the experimental data. The changes in the Avrami parameters indicated that the growth mechanism of curing is mutative. The activation energy calculated with the Avrami equation changed from 65.46 kJ/mol to 25.28 kJ/mol at 180–190 °C, while at 190–200 °C, the activation energy changed from 107.14 kJ/mol to 63.82 kJ/mol. In the model-free analysis, peak separation was achieved due to the change in the curing mechanism. During the prophase of curing with the conversion varying between 0.4 and 0.8, the activation energy increased from 104.3 kJ/mol to 130.6 kJ/mol, as calculated with the Friedman method. Similarly, the activation energy increased from 71.5 kJ/mol to 103.4 kJ/mol when calculated with the integral method. When the conversion exceeded 0.8, the activation energy decreased slightly. The value of the activation energy reduced to 119.4 kJ/mol according to the Friedman method and to 98.2 kJ/mol according to the integral method. The mobility of the reactive groups was hindered because of the high degree of crosslinking density. The kinetics of curing became diffusion controlled. The SiO_2 particles anchored in the net structure physically inhibited the segmental motion. The increase in the activation energy may be attributed to the hindrance effect caused by nano-SiO_2.

Acknowledgements

The authors greatly acknowledge the funds provided by the National Natural Science Foundation of China (Grant No. 51603094), the Postdoctoral Research Support Program of the Jiangsu Province (2019K009), the Postdoctoral Researchers Fund of the Jiangsu Province (2019Z122), the China Postdoctoral Science Foundation (2019M661764) and the Natural Science Foundation of the Jiangsu Province (Grant No. BK20160562).

5 REFERENCES

[1] H. F. Seibert, PMI foam cores find further applications, Reinforced Plastics, 44 (**2000**) 1, 36–38, doi:10.1016/S0034-3617(00)86485-1

[2] H. F. Seibert, Applications for PMI foams in aerospace sandwich structures, Reinforced Plastics, 50 (**2006**) 1, 44–48, doi:10.1016/S0034-3617(06)70873-6

[3] Y. Chen, Preparation and structural characterization of polymethacrylimide foams, New Chemical Materials, 35 (**2007**) 2, 32–34, doi:10.2514/1.26230

[4] J. Qu, D. Ju, Research on the dynamic mechanical properties of polymethacrylimide foam sandwich structure, Composite Structures, 204 (**2018**) 22–30, doi:10.1016/j.compstruct.2018.07.078

[5] T. Chen, G. Zhang, X. Zhao, Structure and properties of AN/MAA/AM copolymer foam plastics, Journal of Polymer Research, 17 (**2009**) 2, 171–181, doi:10.1007/s10965-009-9303-x

[6] P. V. Kornienko, Y. P. Gorelov, K. V. Shirshin, Preparation of foamed polymethacrylimide structural materials from cross-linked copolymers of acrylonitrile and methacyrlic acid, Russian Journal of Ap-

plied Chemistry, 85 (**2012**) 11, 1748–1752, doi:10.1134/s1070427212110195

[7] T. Liu, G. Zhang, Mechanical properties of methacylic acid/acrylonitrile copolymer foam, Polymer Engineering and Science, 47 (**2007**) 3, 314–322, doi:10.1002/pen.20710

[8] H. Y. Tang, X. B. Rao, Effects of multiple crosslinking agents on structure and properties of polymethacrylimide (PMI) foams, Materials Research Innovations, 18 (**2014**) sup2, 473–477, doi:10.1179/1432891714z.000000000447

[9] T. M. Liu, Y. S. Zheng, Application of Photo Initiation Copolymerization during the Preparation of Polymethacrylimide Copolymer Foam, Journal of Applied Polymer Science, 112 (**2010**) 5, 3041–3047, doi:10.1002/app.29896

[10] M. John, T. Skala, Dimensional Changes in CFRP/PMI Foam Core Sandwich Structures, Applied Composite Materials, 20 (**2013**) 4, 601–614, doi:10.1007/s10443-012-9288-1

[11] L. D. Mcgarva, B. T. Astrom, Experimental investigation of compression moulding of glass/PA12-PMI foam core sandwich components, Composites Part A: Applied Science and Manufacturing, 30 (**1999**) 10, 1171–1185, doi:10.1016/S1359-835X(99)00028-7

[12] F. Yang, Q. Y. Lin, J. J. Jiang, Experimental study on fatigue failure and damage of sandwich structure with PMI foam core, Fatigue & Fracture of Engineering Materials & Structures, 38 (**2015**) 4, 456–465, doi:10.1111/ffe.12246

[13] M. Rinker, M. John, Face sheet debonding in CFRP/PMI sandwich structures under quasi-static and fatigue loading considering residual thermal stress, Engineering Fracture Mechanics, 78 (**2011**) 17, 2835–2847, doi:10.1016/j.engfracmech.2011.07.007

[14] I. Choi, J. G. Kim, Radar absorbing sandwich construction composed of CNT, PMI foam and carbon/epoxy composite, Composite Structures, 94 (**2012**) 9, 3002–3008, doi:10.1016/j.compstruct.2012.04.009

[15] J. T. Siivola, S. Minakuchi, N. Takeda, Effect of temperature and humidity conditions on polymethacrylimide (PMI) foam core material and indentation response of its sandwich structures, Journal of Sandwich Structures and Materials, 17 (**2015**) 4, 335–358, doi:10.1177/1099636215570831

[16] Z. Zhang, M. Xu, B. Li, Research on rapid preparation and performance of polymethacrylimide foams, Journal of Applied Polymer Science, 134 (**2017**) 24, doi:10.1002/app.44959

[17] Y. Chen, The polymethacrylimide foam/inorganic nanocomposite and its preparation method, Green Chemistry, 22 (**2008**) 17, 5722–5729

[18] L. Yan, W. Jiang, Enhancement by Metallic Tube Filling of the Mechanical Properties of Electromagnetic Wave Absorbent Polymethacrylimide Foam, Polymers, 11 (**2019**) 2, 372, doi:10.3390/polym11020372

[19] S. Ghiyasi, M. G. Sari, Hyperbranched poly(ethyleneimine) physically attached to silica nanoparticles to facilitate curing of epoxy nanocomposite coatings, Progress in Organic Coatings, 120 (**2018**) 1, 100–109, doi:10.1016/j.porgcoat.2018.03.019

[20] Y. Nakamura, M. Yamaguchi, Effects of particle size on mechanical and impact properties of epoxy resin filled with spherical silica, Journal of Applied Polymer Science, 45 (**1992**) 7, 1281–1289, doi:10.1002/app.1992.070450716

[21] M. Jouyandeh, O. M. Jazani, High-performance epoxy-based adhesives reinforced with alumina and silica for carbon fiber composite/steel bonded joints, Journal of Reinforced Plastics and Composites, 35 (**2016**) 23, 1685–1695, doi:10.1177/0731684416665248

[22] Z. Zhang, M. Xu, B. Li, Preparation and characterization of polymethacrylimide/silicate foam, Polymers for Advanced Technologies, 29 (**2018**) 12, 2982–2991, doi:10.1002/pat.4418

[23] F. Tikhani, M. Jouyandeh, Cure Index demonstrates curing of epoxy composites containing silica nanoparticles of variable morphology and porosity, Progress in Organic Coatings, 135 (**2019**) 176–184, doi:10.1016/j.porgcoat.2019.05.017

[24] M. Jouyandeh, O. M. Jazani, Surface engineering of nanoparticles with macromolecules for epoxy curing: Development of super-reactive nitrogen-rich nanosilica through surface chemistry manipulation, Applied Surface Science, 447 (**2018**) 152–164, doi:10.1016/j.apsusc.2018.03.197

[25] G. Kortaberria, L. Solar, Curing of an epoxy resin modified with nanoclay monitored by dielectric spectroscopy and rheological measurements, Journal of Applied Polymer Science, 102 (**2006**) 6, 5927–5933, doi:10.1002/app.25108

[26] B. Lucio, J. L. de la Fuente, Non-isothermal DSC and rheological curing of ferrocene-functionalized, hydroxyl-terminated polybutadiene polyurethane, Reactive & Functional Polymers, 107 (**2016**) 60–68, doi:10.1016/j.reactfunctpolym.2016.08.002

[27] M. R. Saeb, H. Rastin, Cure kinetics of epoxy/MWCNTs nanocomposites: Nonisothermal calorimetric and rheokinetic techniques, Journal of Applied Polymer Science, 134 (**2017**) 35, doi:10.1002/app.45221

[28] K. P. Menard, N. R. Menard, Dynamic Mechanical Analysis in the Analysis of Polymers and Rubbers, ACS Applied Materials & Interfaces, 12 (**2015**) 33, 37607–37618, doi:10.1002/0471440264.pst102.pub2

[29] Y. Yuan, C. Dazhu, Cure behavior of epoxy resin/CdS/2,4-EMI nanocomposites investigated by dynamic torsional vibration method (DTVM), Polymer Bulletin, 57 (**2006**) 2, 219–230, doi:10.1007/s00289-006-0550-2

[30] J. Zhang, R. Ye, A Study of Isothermal Curing of PMI Using DMA, Advances in Materials Science and Engineering, 2015 (**2015**) 1–12, doi:10.1155/2015/695286

[31] S. Dalton, F. Heatley, P. M. Budd, Thermal stabilization of polyacrylonitrile fibres, Polymer, 40 (**1999**) 20, 5531–5543, doi:10.1016/S0032-3861(98)00778-2

[32] L. Nunez, F. Fraga, Effects of diffusion on the kinetic study of an epoxy system diglycidyl ether of bisphenol A/1,2-diamine cyclohexane/calcium carbonate filler, Journal of Applied Polymer Science, 77 (**2000**) 10, 2285–2295, doi:10.1002/1097-4628(20000906)77:10<2285::AID-APP22>3.0.CO;2-W

[33] S. Montserrat, C. Flaque, Effect of the crosslinking degree on curing kinetics of an epoxy–anhydride system, Industrial Crops and Products, 117 (**1995**) 169–178, doi:10.1002/app.1995.070561104

[34] S. Khostavan, A. Omrani, A. A. Rostami, Influence of multiwalled carbon nanotubes on reaction kinetics of epoxy cured with 1,4-bis (3-aminopropoxy) butane, Monatshefte für Chemie – Chemical Monthly, 144 (**2013**) 2, 147–153, doi:10.1007/s00706-012-0774-9

[35] Y. Li, K. Luo, Performance improvement of a p-Cu_2O nanocrystal photocathode with an ultra-thin silver protective layer, Chemical Communications, 55 (**2019**) 67, 9963–9966, doi:10.1039/C9CC04994K

[36] J. Zhang, C. Zhang, S. A. Madbouly, In situ polymerization of bio-based thermosetting polyurethane/graphene oxide nanocomposites, Journal of Applied Polymer Science, 132 (**2015**) 13, doi:10.1002/app.41751

[37] H. S. Y. Hsich, Kinetic model of cure reaction and filler effect, Journal of Applied Polymer Science, 27 (**1982**) 9, 3265–3277, doi:10.1002/app.1982.070270907

[38] M. G. Lu, M. J. Shim, S. W. Kim, Dynamic DSC Characterization of Epoxy Resin by Means of the Avrami Equation, Journal of Thermal Analysis and Calorimetry, 58 (**1999**) 3, 701–709, doi:10.1023/A:1010177116739

[39] J. J. Jonas, X. Quelennec, The Avrami kinetics of dynamic recrystallization, Acta Materialia, 57 (**2009**) 9, 2748–2756, doi:10.1016/j.actamat.2009.02.033

[40] H. Rastin, M. R. Saeb, Transparent nanocomposite coatings based on epoxy and layered double hydroxide: nonisothermal cure kinetics and viscoelastic behavior assessments, Green Chemistry, 21 (3), 526–537, doi:10.1016/j.porgcoat.2017.09.003

[41] S. Sahoo, H. Kalita, Meticulous study on curing kinetics of green polyurethane-clay nanocomposite adhesive derived from plant oil:

Evaluation of decomposition activation energy using TGA analysis, Journal of Macromolecular Science, Part A, 54 (**2017**) 11, 819–826, doi:10.1080/10601325.2017.1336727

[42] A. L. Daniel-da-Silva, J. C. M. Bordado, J. M. Martín-Martínez, Moisture curing kinetics of isocyanate ended urethane quasi-prepolymers monitored by IR spectroscopy and DSC, Journal of Applied Polymer Science, 107 (**2010**) 2, 700–709, doi:10.1002/app.26453

[43] S. Vyazovkin, Evaluation of activation energy of thermally stimulated solid-state reactions under arbitrary variation of temperature, Journal of Computational Chemistry, 18 (**1997**) 3, 393–402, doi:10.1002/(sici)1096-987x(199702)18:3<393::aid-jcc9>3.0.co;2-p

[44] S. Vyazovkin, C. A. Wight, Model-free and model-fitting approaches to kinetic analysis of isothermal and nonisothermal data, Thermochimica Acta, 340–341 (**1999**) 1, 53–68, doi:S0040-6031(99)00253-1

[45] T. Ozawa, Kinetic analysis of derivative curves in thermal analysis, Journal of Thermal Analysis and Calorimetry, 2 (**1970**) 3, 301–324, doi:10.1007/bf01911411

[46] S. Vyazovkin, N. Sbirrazzuoli, Kinetic analysis of isothermal cures performed below the limiting glass transition temperature, Macromolecular Rapid Communications, 21 (**2000**) 2, 85–90, doi:10.1002/(SICI)1521-3927(20000201)21:2<85::AID-MARC85>3.0.CO;2-G